

PACS numbers: 42.79.Bh; 52.50.Jm; 52.38.Ph
DOI: 10.1070/QE2009v039n05ABEH013902

Measurements of reflection spectra of soft X-ray multilayer mirrors using a broadband laser-plasma radiation source

E.A. Vishnyakov, K.N. Mednikov, A.A. Pertsov, E.N. Ragozin,
A.A. Reva, A.S. Ul'yanov, S.V. Shestov

Abstract. **The reflection spectra of several concave (spherical and parabolic) periodic Mo/Si, Mg/Si, and Al/Zr multilayer mirrors intended for cosmic experiments were studied with the help of a laser-plasma soft X-ray radiation source. An investigation was made of the reflection spectra of a laboratory aperiodic Mo/Si multilayer mirror optimised for maximum uniform reflectivity in the 125 – 250-Å range. 'Satellites' were observed in the neighbourhood of the principal peak in the spectrum of the periodic 132-Å multilayer mirror. High-intensity second-order interference reflection peaks at wavelengths of about 160 Å were experimentally revealed in the reflection spectra of the periodic Mo/Si 304-Å mirrors. By contrast, the second-order reflection peak is substantially depressed in the spectra of the narrow-band mirrors based on the Mg/Si multilayer structure. The experimental data are compared with theoretical calculations. Manifestations of the NEXAFS structure of the $L_{2,3}$ absorption edges of Al and Al_2O_3 were observed in the spectra recorded.**

Keywords: *laser-plasma radiation source, soft X-ray range, imaging (stigmatic) diffraction spectrometer, normal-incidence soft X-ray multilayer mirrors, NEXAFS L-edge absorption structure of Al.*

1. Introduction

At present, soft X-ray multilayer optics has become an inherent part of experiments which involve radiation recording and the diagnostics of laboratory and astrophysical plasmas. Contemporary advances in the solar astronomy of soft X-ray (SXR) and vacuum ultraviolet (VUV) spectral ranges (3 – 60 nm) are related to a considerable extent to the progress in the development of new types of reflective multilayer coatings for X-ray optical elements. Periodic multilayer mirrors (MMs) exhibit a highly selective spectral reflectivity, with the result that they are commonly employed for selecting certain lines or line arrays in line spectra.

In the pursuance of experiments under laboratory conditions there exists a demand for SXR diffraction spectrometers which simultaneously possess stigmatism, a relatively large acceptance angle ($\sim 5 \cdot 10^{-2}$ rad $\times$ $5 \cdot 10^{-2}$ rad), and a rather broad operating spectral range (of the order of an octave or broader) for a resolving power $\lambda/\delta\lambda \sim 3 \times 10^2$ and higher. A stigmatic (imaging) spectroscopic instrument of this kind is realised with the use of aperiodic normal-incidence multilayer mirrors [1 – 4] in combination, for instance, with a transmission diffraction grating.

Periodic X-ray multilayer mirrors are commonly characterised by the peak reflectivity (i.e., the reflectivity at a wavelength $\lambda_0 = 2d\langle n\rangle\cos\theta$, where d is the period of a multilayer structure, $\langle n\rangle$ is the period-averaged refractive index, and θ is the angle of incidence), as well as by the shape and width of the resonance reflection peak. In this case, of practical importance are other parameters of the mirrors as well, which ordinarily go unheeded. The case in point is, for instance, low attendant peaks (the so-called satellites) and higher-order interference reflection peaks, which can make substantial contributions to the reflected radiation flux integrated over the spectrum. The use of a broadband laser-plasma SXR radiation source enables exposing these mirror features and investigating their role in the formation of the reflection signal.

The aim of our work is to study the aforementioned features of the reflection spectra of new-generation periodic MMs developed and synthesised in the Institute for Physics of Microstructures of the Russian Academy of Sciences in the framework of the TESIS/CORONAS-FOTON Project for imaging solar spectroscopy, as well as to study the spectral reflectivity of a broadband aperiodic MM intended for the spectroscopy and diagnostics of laboratory (including laser-produced) plasmas, which was synthesised in the National Technical University 'Kharkov Polytechnic Institute' (Ukraine). For periodic MMs we determined their uniformity over aperture and also estimated the relative role of reflectivity 'wings' with consideration for specific radiation detectors and absorption filters. When investigating the aperiodic MM optimised for maximum uniform reflectivity over some wavelength range, emphasis was placed on its reflectivity variations within the optimisation domain.

2. Experimental setup

Figure 1a shows schematically the optical layout of the imaging (stigmatic) diffraction spectrometer employed in

E.A. Vishnyakov, K.N. Mednikov, A.A. Pertsov, A.A. Reva, A.S. Ul'yanov, S.V. Shestov P.N. Lebedev Physics Institute, Russian Academy of Sciences, Leninsky prosp. 53, 119991 Moscow, Russia;
E.N. Ragozin P.N. Lebedev Physics Institute, Russian Academy of Sciences, Leninsky prosp. 53, 119991 Moscow, Russia; Moscow Institute of Physics and Technology (State University), Institutskii per. 9, 141700 Dolgoprudnyi, Moscow region, Russia;
e-mail: enragozin@sci.lebedev.ru

Received 30 April 2008; revised received 2 October 2008
Kvantovaya Elektronika **39** (5) 474 – 480 (2009)
Translated by E.N. Ragozin

experiments, in which the role of the focusing element was played by the mirrors under study. The spectrometer [5] was assembled on an optical table measuring 0.6 m by 3.6 m in the IKAR vacuum chamber and comprised an entrance slit, an MM under investigation, a wide-aperture transmission diffraction grating, and a detector.

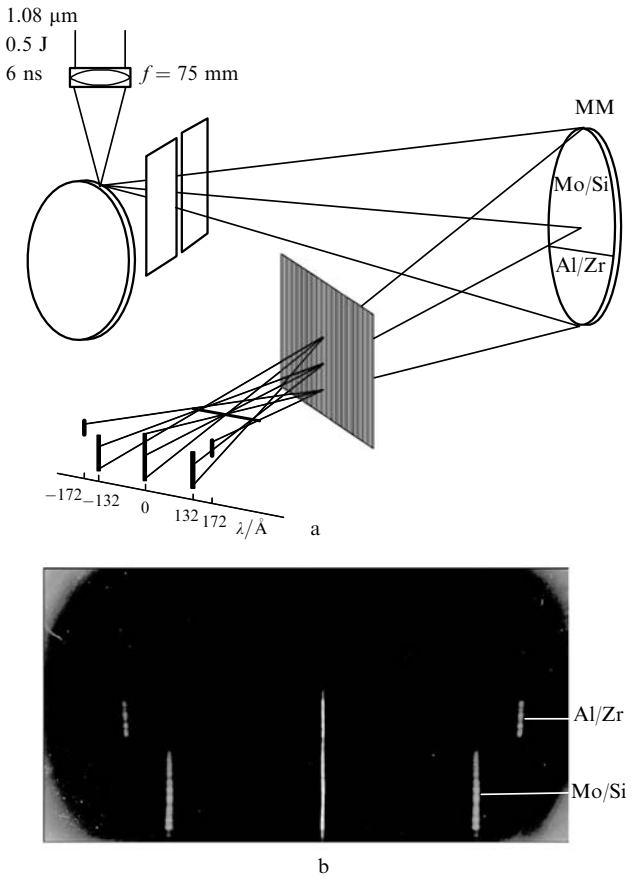

Figure 1. Optical layout of the experiments shown by the example of a spectrometer with a two-sectional MM (Mo/Si and Al/Zr) as the focusing element (a) and reflection spectrum of this MM (b).

According to the Rowland mount, the entrance slit and the recording device were arranged symmetrically about the normal to the surface of the mirror under study passing through the point of incidence of the central ray. The distance between the detector midpoint and the entrance slit was invariable (210 mm), while the radii of curvature of the mirrors under study lay in the 1–3.25-m range. Therefore, the radiation was reflected from the MMs at small (0.1–0.03 rad) angles of incidence. As a result, aberrations of the setup were quite small and the spectral images of the entrance slit produced by the multilayer mirrors on the sensitive surface of a detector were highly stigmatic. The spectral slit width depended on the grating–detector separation and was equal to 1.5–3 Å in different measurements.

In our setup, the function of an SXR source was fulfilled by the plasma produced under the irradiation of a tungsten target by the nanosecond pulses of a neodymium-doped yttrium orthoaluminate crystal laser ($Nd:YAlO_3$, 0.5 J, 6 ns, 1.08 μm). The laser beam was focused on the target in a spot with an effective area $S_{eff} \sim 10^{-5}$ cm^2 using a heavy flint lens with a focal length $f = 75$ mm. The peak laser radiation intensity at the centre of the focal spot was $\sim 10^{13}$ W cm^{-2}.

As is well known [6, 7], owing to the high atomic number of tungsten the generated plasma radiation possesses a quasi-continuous spectrum with an intensity smoothly varying in the 20–350-Å range. This permits using this radiation for research in a rather broad spectral range. The resultant intensity of each of the spectra recorded in this work is equal to the product of the intensity of the slowly varying source spectrum, the reflectivity of the mirror under investigation, and detector responsivity (with the inclusion of the filter transmittance).

The entrance slit was located at a distance of either 110 or 20 mm from the laser focal spot on the target, depending on the radius of the MM curvature. The slit width was 45 μm and was kept invariable from experiment to experiment. In each individual measurement, the entrance slit and the detector were mounted on the Rowland circle of a concave MM under study.

A free-standing wide-aperture transmission diffraction grating (1000 lines mm^{-1}, 5 cm^2) was placed in the path of the beam reflected from the MM under study; the detector–grating distance was selected in such a way that the plate scale was equal to the requisite value. The sensitive detector elements were two backside-illuminated E2V CCD 47-10 matrices with a pixel size of 13 μm; one of them was coated with an Al layer and the other with a multilayer Zr/Si structure. The deposited coatings fulfilled the function of absorption filters.

Due to the small dimensions of the laser-plasma source (~ 0.05 mm), the radiation emanating from some point of the entrance slit illuminated a relatively small (1–3 mm vertically) portion of the MM aperture. That is why such a portion of the aperture formed a horizontal strip of the spectral image at a specific height on the detector. All the strips taken together formed a vertically extended spectrum. The dependence of the shape of the spectrum on the vertical coordinate on the detector therefore enables judging the uniformity of the multilayer coating over the aperture of a MM under study. In particular, a variation of the distance between the corresponding portions of the spectral image and the zero diffraction order is indication that the multilayer structure period depends on the coordinate of a point on the mirror aperture.

3. Features of the spectra recorded

In the course of the work we measured the spectral characteristics of several periodic SXR multilayer mirrors, some of which were two-sectional (the aperture was divided into two segments, on which different multilayer coatings were deposited). Collected in Table 1 are the tentative data about all the MMs whose spectra are given in this paper.

3.1 Multilayer coating nonuniformity over apertures of the mirrors under study

Figure 1b shows the reflection spectrum of a two-sectional (Mo/Si and Al/Zr) MM, whose reflection peaks should fall on wavelengths of 132 and 172 Å. One can see that the spectral lines of the 172-Å fragment are slightly inclined, which is indication that the multilayer structure period increases towards the edge of the MM aperture (in this case, the reflectivity peak shifts from 172 to 176 Å). The $\lambda_0 \approx$ 132-Å fragment exhibits inclination-free spectral lines,

Table 1. Main parameters of the multilayer mirrors under study.

λ_0/Å	Material	Shape	Radius of curvature/mm	Number of monolayers	Period/Å
132/172	Mo/Si, Al/Zr	Parabolic	3250	100, 100	68, 87
192	Mo/Si	Spherical	1612	80	98
132	Mo/Si	Parabolic	3250	100	68
304	Mo/Si	Parabolic	1000	30	166
304	Mo/Si	Parabolic	1200	24	164
304	Mg/Si	Parabolic	3250	80	157
Broadband mirror	Mo/Si	Spherical	1000	80	–

Note: specified for parabolic mirrors is the radius of curvature at the apex.

which testifies to the uniformity of the multilayer structure period over the aperture of the fragment.

Another example of a weakly nonuniform MM is provided by a periodic Mo/Si MM, whose reflection peak should occur at $\lambda_0 \approx 192$ Å; its spectrum is depicted in Fig. 2. As is clear from Fig. 2, the edges of the spectral line are more distant from the zero diffraction order than its middle part. The MM reflectivity peak shifts from 190 Å at the centre to 194 Å at the edges of the aperture. This is testimony that the multilayer structure period at the edges of the mirror is approximately 2 Å longer than at the centre.

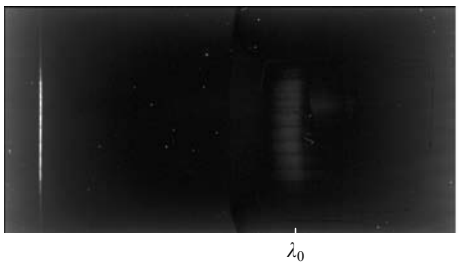

Figure 2. Reflection spectrum of a periodic $\lambda_0 = 192$-Å Mo/Si mirror.

The reflection spectra of the remaining periodic MMs are indicative of the high aperture uniformity of their multilayer coatings.

3.2 Satellites about the principal reflection peak ($\lambda_0 = 132$-Å MM)

In the spectrum of a periodic Mo/Si mirror with a $\lambda_0 \approx 132$-Å reflection peak, one can clearly see satellites on either side of the principal peak (Figs 3a and 3b). In the long-wavelength domain these satellites are greater in number and are clearer visible. This is in perfect agreement with the data of numerical calculations [1] (Fig. 3c), the spacing between the satellites in the spectrum being determined by the total number of layers in the multilayer structure. The theoretical calculation was performed for 100 monolayers of Mo and Si and took into account the existence of transition layers. The structure period was taken to be 68.6 Å and the Mo fraction in the period was 29.4 % in thickness.

It is pertinent to note that for transition layers we employed 12-Å thick Mo-on-Si layers and 6-Å-thick Si-on-Mo layers with the stoichiometry of molybdenum silicide $MoSi_2$ in all numerical calculations of the Mo/Si multilayer

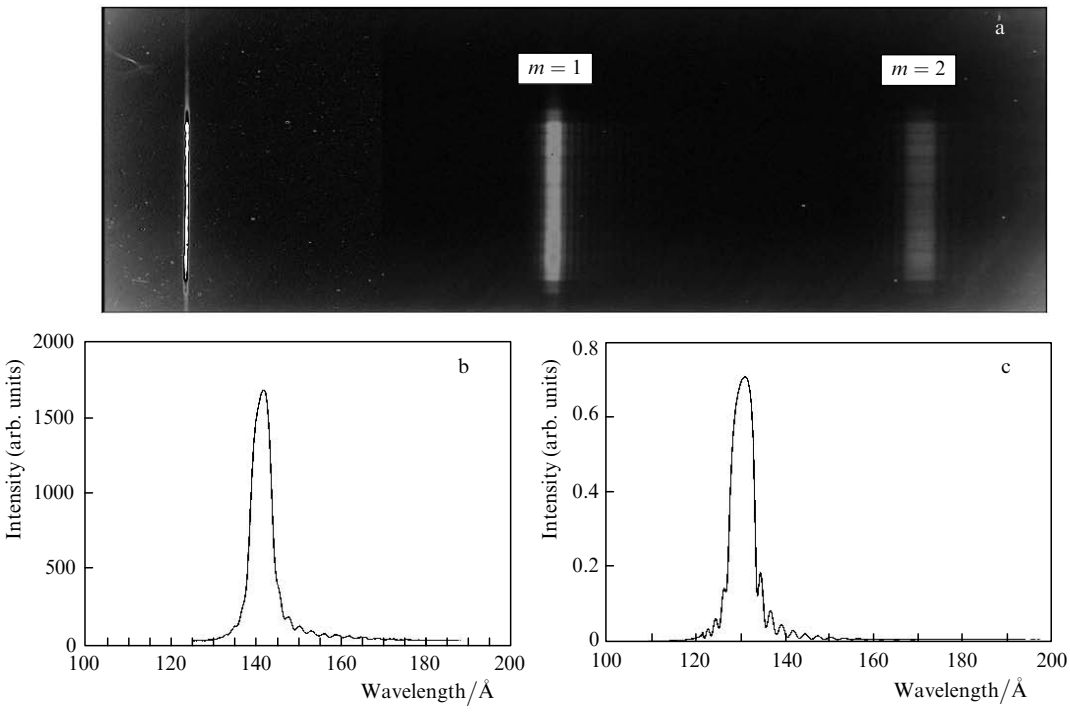

Figure 3. Reflection spectrum of a $\lambda_0 \approx 132$-Å MM (a, b) and spectrum calculated theoretically with the inclusion of 100 monolayers (c) ($m = 1, 2$ – the first and second diffraction orders).

structures described in this work. The optical material constants for all numerical calculations were borrowed from Ref. [8].

A comparison of the experimental and calculated curves (Figs 3b and 3c) allows assessing the resolving power of the setup under description as well as the quality of the periodic structure of the MM. We notice that all satellites except the first one are resolved in the experimental spectrum. This is confirmation that the spectral resolution of the setup was 1.2 Å. On the other hand, the close resemblance between the experimental spectrum and the calculated one, both in the shape of the principal peak and the satellite array, emphasise the high quality of the periodic structure of the MM under investigation.

3.3 Second-order interference peak of $\lambda_0 \approx 304$-Å MMs

In the present work we measured the reflection spectra for two types of multilayer mirrors having reflection peaks near 304 Å. The case in point is mirrors based on the 'classical' Mo/Si structure and a new periodic Mg/Si structure.

Earlier reported was the synthesis of Mg/SiC multilayer structures with reflectivities of 30 % – 40 % at a wavelength of $\sim$ 304 Å [9]. The high efficiency of the Mg/Si multilayer structure for the operation with $\sim$ 304-Å radiation was predicted in Ref. [10], but this structure was not synthesised. In our work we investigated the MMs synthesised on the basis of the Mg/Si structure involving Cr and B_4C buffer layers [11].

There is good reason to compare the calculated reflection coefficients for the Mo/Si and Mg/Si structures in the 100 – 350-Å wavelength range (Fig. 4). The reflection coefficient for the Mg/Si structure was calculated without the inclusion of the buffer layers, while for Mo/Si the effect of transition layers was taken into account. In the calculation of the Mo/Si structure its period was equal to 165 Å and the content of Mo in the period was 18.7 %. The Mg/Si structure period was equal to 157 Å and the Mg fraction was 68 % in thickness.

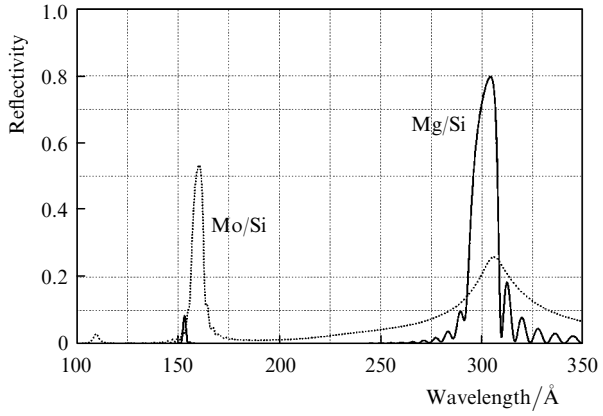

Figure 4. Calculated reflection coefficients of the Mg/Si (continuous curve) and Mo/Si (dotted curve) multilayer structures with $\lambda_0 = 304$ Å.

In the calculated spectrum of the Mo/Si multilayer structure there is a second-order interference peak at a wavelength near 160 Å, which exhibits a strongly pronounced intensity. Because the average refractive index of the Mo/Si structure increases as the wavelength becomes shorter, the second interference peak shifts slightly towards longer wavelengths and peaks at a wavelength of about 160 Å rather than at 152 Å. Furthermore, the first-order peak is characterised by a large width at half maximum (30 – 35 Å) and broad 'wings'. These two circumstances are a substantial complication in the spectroscopic analysis of undispersed images obtained using such a multilayer mirror.

Also plotted in Fig. 4 is the calculated reflection coefficient for the new Mg/Si multilayer structure. Near a wavelength of 250 Å there lies the L absorption edge of Mg, which possesses a substantially lower absorption in the $\sim$ 300-Å domain in comparison with Mo. Owing to the use of Mg in the multilayer structure, first, there 'operates' a several-fold greater number of layers, which makes the resonance reflection peak much narrower, and, second, the second-order interference reflection peak is substantially suppressed, because it occurs far beyond the L absorption edge of Mg. Therefore, the Mg/Si-based MMs are devoid of both of the above features inherent in Mo/Si mirrors, and they are the mirrors of choice for recording quasi-monochromatic spectral images in the spectral region involved.

Figure 5 shows the experimental reflection spectra for MMs with peaks near 304 Å. The second diffraction orders of the near-160-Å peaks, which are partly superimposed on the spectra in the neighbourhood of 320 Å, are removed from the spectra of the Mo/Si mirrors given in Fig. 5. As would be expected, the spectra of the Mo/Si multilayer structures exhibit clearly the second-order interference reflection peak, while the principal (first-order) reflection peak possesses a large width at half maximum ($\sim$ 30 Å). At the same time, the Mg/Si-mirror spectrum possesses a rather narrow ($\sim$ 12 Å) principal reflection peak, while the reflection near $\lambda = 160$ Å is hardly present, which is also consistent with the theory.

3.4 Variations in the spectral reflectivity of an aperiodic MM

In the course of experiments we measured the reflection spectra of an aperiodic laboratory MM optimised for maximum uniform reflectivity in the 125 – 250-Å range. Initially the MM reflection spectrum was recorded with the Zr/Si-filter coated CCD (Fig. 6) and then, without any modifications of the layout, with the Al-filter coated CCD (Fig. 7).

The short-wavelength bound of both spectra is defined by the respective L absorption edges of Si and Al, while the long-wavelength bound is due to a decrease in the intensity of the emission spectrum of the tungsten plasma as well as to a lowering in Zr transmission in the case of the Zr/Si-filter coated detector. Proceeding from the spectra obtained, we can therefore judge with certainty the reflectivity variations of this MM only in the 125 – 190-Å wavelength range. On the basis of the spectrum shown in Fig. 6b it is valid to say that the reflectivity variations in this broadband aperiodic MM amount to about $\pm$15 % in this spectral domain.

4. Manifestation of NEXAFS structure of the L absorption edge of Al in the spectra recorded

4.1 $L_{2,3}$ absorption edge of Al in the spectra of the $\lambda_0 = 304$-Å MMs

All spectra of the multilayer mirrors with reflection peaks centred near a wavelength of 304 Å were recorded with the Al-filter coated CCD. As is well known, the $L_{2,3}$ absorption

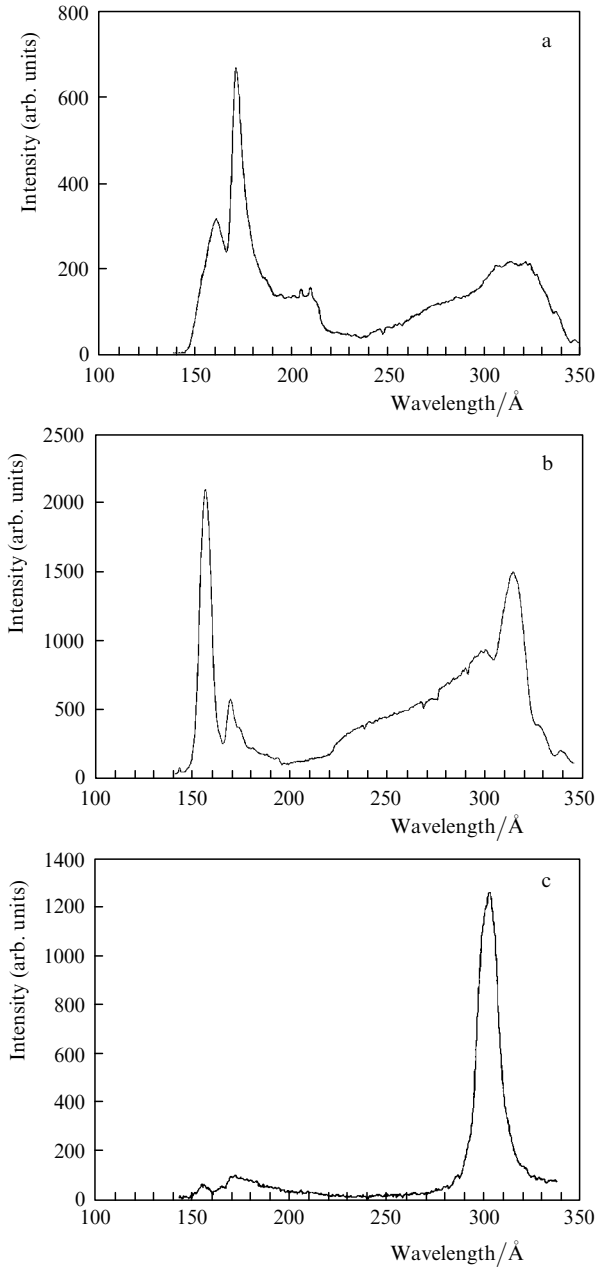

Figure 5. Reflection spectra of the MMs intended for the reflection of $\lambda = 304$-Å radiation for previous-generation Mo/Si mirrors (a, b) and Mg/Si mirrors with $\lambda_0 = 304$ Å (c).

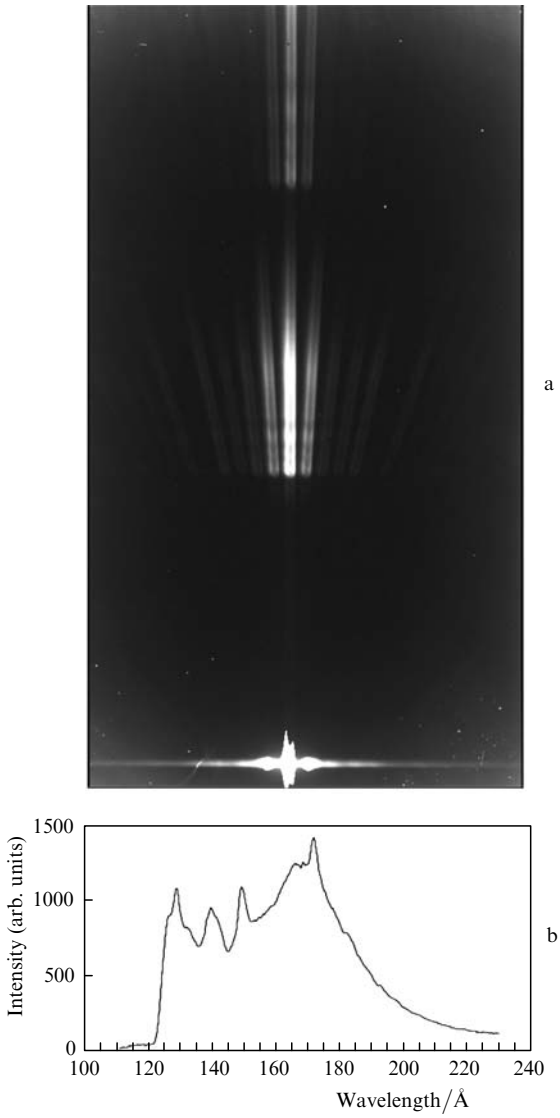

Figure 6. Reflection spectrum of an aperiodic laboratory MM optimised for maximum uniform reflectivity in the 125–250-Å range, which was recorded using the Zr/Si-filter coated detector (a), and its graphic representation (b).

edge of Al is located at a wavelength of ~ 170 Å. One would therefore think that the $\lambda = 160$-Å reflection peak should not show up in the recorded spectra of the Mo/Si multilayer mirrors. However, from the experimental data there emerges an entirely different picture.

Figure 5 shows the reflection spectra of two Mo/Si mirrors and one Mg/Si mirror. The Mo/Si-based mirrors (Figs 5a and 5b) possess reflection peaks at wavelengths of 310–315 Å. Because of this, their second-order interference peaks ($\lambda \approx 160$ Å) are shifted still further to the long-wavelength side in comparison with the mirror having a reflection peak at $\lambda_0 = 304$ Å. That is why they lie in part above the $L_{2,3}$ absorption edge of Al (i.e., in the $\lambda > 170$-Å domain). However, even those parts of the peaks which are below the edge (for $\lambda < 170$ Å) are clearly visible in the spectrum. From Fig. 5 it follows that the spectra do exhibit a dip, beginning from 170 Å. However, at wavelengths of ~ 160 Å, i.e. already below the L edge, the signal becomes stronger again. It is likely that these spectra manifest the so-called fine structure of the $L_{2,3}$ absorption edge of Al, which is also referred to as NEXAFS (Near-Edge X-Ray Absorption Fine Structure), or XANES (X-Ray Absorption Near-Edge Structure). Now let us consider the reflection spectra of Mg/Si-based mirrors (Fig. 5c). The reflection spectra of both MMs with this kind of multilayer structure turned out to be perfectly similar, and so only one of them is reproduced in the Figure. Since the L absorption edge of Al lies near $\lambda = 250$ Å, reflection in the $\lambda \sim 160$-Å region is hardly visible in the spectra recorded. However, the fine structure of the $L_{2,3}$ absorption edge of Al may be traced even in these spectra.

4.2 Manifestation of the L absorption edge of Al in the spectrum of the broadband aperiodic MM

Using the reflection spectra of the broadband aperiodic MM it has been possible to vividly illustrate the manifes-

tation of the NEXAFS for the $L_{2,3}$ absorption edge of Al. One can clearly see from Fig. 7 that there are regions of partial wavelength-dependent transmission below the $L_{2,3}$-edge of Al. The low-transmittance region can be traced down to ~ 130 Å.

If we take the direction of decreasing wavelength in Fig. 7, at $\lambda = 170$ Å there begins a sharp decease in intensity, which terminates at $\lambda \approx 167$ Å. The intensity remains approximately constant down to $\lambda \approx 162$ Å, and then begins to lower again to attain a minimum at $\lambda = 157 - 158$ Å. Next, the intensity has a peak at $\lambda = 154$ Å followed by a decrease to $\lambda = 135$ Å, with a minimum visible at $\lambda = 145$ Å. We give a plausible explanation of this behaviour of the spectral intensity.

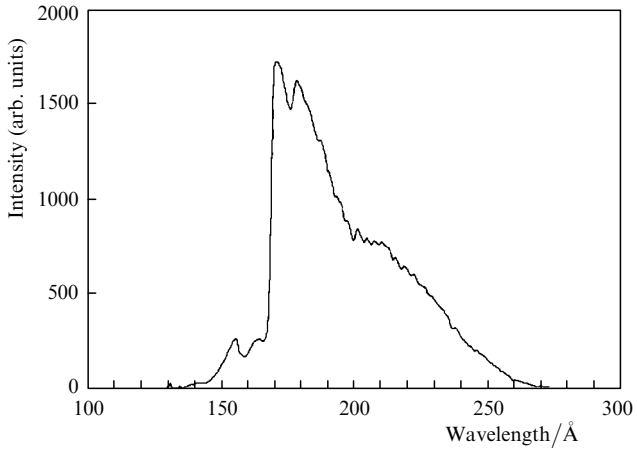

Figure 7. Reflection spectrum of the aperiodic laboratory MM recorded using the Al-coated CCD.

Codling and Madden [12] studied the transmittance of the films of amorphous and crystalline Al_3O_3. According to their assertion, owing to the chemical bond the L-edge of Al_3O_3 lies not at a wavelength $\lambda \approx 170$ Å but at $\lambda \approx 162$ Å for amorphous Al_3O_3 and at $\lambda \approx 160$ Å for crystalline Al_2O_3. Both wavelength dependences of Al_2O_3 transmittance are given in Ref. [12].

Gahwiller and Brown [13] give the absorption coefficient of practically pure Al as a function of photon energy in the 70 – 190-eV range. They noted strong absorption peaks at $\lambda = 129$ Å and 106 Å (the L_1-edge of Al) as well as weaker absorption peaks at $\lambda = 147$ and 111 Å. The absorption of pure Al is hardly changed in the 73 – 80-eV (170 – 155 Å) range.

On the basis of the data given in Refs [12, 13] and considering the reflection spectrum of the aperiodic mirror in the range shown in Fig. 6b, the following can be said about the spectrum given in Fig. 7. The fall in intensity at $\lambda \approx 170$ Å is due to pure Al in the filter coating. The same underlies the approximate intensity uniformity in the 167 – 162-Å domain. Next, the intensity begins to decrease again down to $\lambda \approx 157$ Å. This is partly attributable to the lowering in the reflectivity of the aperiodic MM (Fig. 6b) and partly to a lowering in Al2O3 film transmittance. Next the intensity increases to exhibit a maximum at $\lambda = 154$ Å. This may be attributed to a sharp rise in Al_3O_3 transmittance near $\lambda \approx 154$ Å [12].

The fall of intensity after $\lambda \approx 154$ Å is due to the combined effect of a decrease in transmission both for pure aluminium and for Al_3O_3 in the 154 – 147-Å domain. Furthermore, an appreciable lowering in the reflectivity of the aperiodic mirror is observed in the 149 – 145-Å region (Fig. 6b), which is of first importance in this case. This may explain the occurrence of intensity minimum at $\lambda \approx 145$ Å rather than at $\lambda \approx 147$ Å (Fig. 7). Observed below $\lambda \approx 145$ Å (down to 129 Å) is a rapid increase in the absorption of pure Al, and so the intensity of the spectrum of Fig. 7 is close to zero near $\lambda \approx 130$ Å.

From the aforesaid it may be inferred that the Al absorption filter employed in our work contains pure Al and an Al_2O_3 oxide (most likely, crystalline) film. In this case, from Fig. 7 it is possible to make a rough estimate of the Al-to-Al_2O_3 layer thickness ratio. The Al layer thickness defines the fall of filter transmission at $\lambda \approx 170$ Å, while the Al_2O_3 layer thickness defines the characteristic oscillation scale in the NEXAFS of the L absorption edge, which manifests itself in the recorded spectrum. Taking into account this fact and the exponential nature of absorption, the Al layer thickness in the filter may be estimated at about 0.1 μm. An estimate of the Al_2O_3 layer thickness yields a value smaller by an order of magnitude.

One more circumstance is worthy of mention. The aluminium filter was assumed to contain only pure Al and Al_2O_3. However, in reality this may not be the case. The chemical filter composition is largely determined by its deposition and storage conditions [14]. It turns out that the system 'pure $Al + Al_2O_3$' is never realised in practice, although this is precisely the approximation employed for making crude estimates.

5. Conclusions

We have demonstrated the high efficiency of using a broadband laser-plasma SXR radiation source in combination with a diffraction spectrometer for investigating concave MMs. The spectral characteristics of several imaging multilayer mirrors were evaluated. These measurements showed the high aperture uniformity for the majority of new-generation multilayer mirrors and revealed weak nonuniformities for the MMs of earlier generations. The resultant reflection spectra exhibited the following features.

(i) In the reflection spectrum of a $\lambda_0 = 132$-Å Mo/Si mirror there are satellites, whose spacing is determined by the number of layers in the multilayer structure.

(ii) Mo/Si multilayer mirrors intended for recording radiation in the vicinity of $\lambda = 304$ Å possess high-intensity reflection peaks in the second interference order.

(iii) In comparison with the Mo/Si mirrors, the new Mg/Si-based multilayer structure possesses a high selectivity: a narrow resonance reflection curve ($\lambda_0 \approx 304$ Å, $\delta\lambda_{1,2} \approx 12$ Å), relatively low-intensity 'wings', and a lower reflection coefficient in the second interference order. Owing to these distinctions between the reflection spectra of Mo/Si and Mg/Si periodic structures, MMs synthesised on their basis may find different application. In particular, Mo/Si multilayer mirrors may be used in spectroheliographs, while narrow-band Mg/Si mirrors are the mirrors of choice for use in telescopes intended for forming monochromatic spectral images.

(iv) Manifested in the second-order interference peak in the reflection spectra of both Mo/Si and Mg/Si multilayer structures is the NEXAFS of the $L_{2,3}$ absorption edge of the aluminium absorption filter. The fine structure of the Al L

absorption edge also shows up in the reflection spectrum of the aperiodic laboratory Mo/Si mirror optimised for maximum uniform reflectivity in the 125–250-Å range. From the form of this spectrum we obtained an estimate of Al filter thickness and the ratio between Al Al_2O_3 layer thickness in it.

Acknowledgements. The authors express their appreciation to S.V. Kuzin for his constant interest and encouragement and to A.S. Pirozhkov for placing at our disposal the program for the calculation and optimisation of X-ray multilayer mirrors. This work was supported by the Russian Foundation for Basic Research (Grant Nos 07-02-00316-a and 08-02-01301-a).

References

1. Kolachevskii N.N., Pirozhkov A.S., Ragozin E.N. *Kvantovaya Elektron.*, **30** (5), 428 (2000) [*Quantum Electron.*, **30** (5), 428 (2000)].
2. Ragozin E.N., Kondratenko V.V., Levashov V.E., Pershin Yu.P., Pirozhkov A.S. *Proc. SPIE Int. Soc. Opt. Eng.*, **4782**, 176 (2002).
3. Kapralov V.G., Korde R., Levashov V.E., Pirozhkov A.S., Ragozin E.N. *Kvantovaya Elektron.*, **32** (2), 149 (2002) [*Quantum Electron.*, **32** (2), 149 (2002)].
4. Beigman I.L., Pirozhkov A.S., Ragozin E.N. *J. Opt. A: Pure Appl. Opt.*, **4**, 433 (2002).
5. Zhitnik I.A., Kuzin S.V., Mitropol'skii M.M., Ragozin E.N., Slemzin V.A., Sukhanovskii V.A. *Kvantovaya Elektron.*, **20** (1), 89 (1993) [*Quantum Electron.*, **23** (1), 76 (1993)].
6. Gullikson E.M., Underwood J.H., Batson P.C. *J. X-Ray Sci. Technol.*, **3**, 283 (1992).
7. Kolachevskii N.N., Pirozhkov A.S., Ragozin E.N. *Kvantovaya Elektron.*, **25** (9), 843 (1998) [*Quantum Electron.*, **28** (9), 821 (1998)].
8. Henke B.L., Gullikson E.M., Davis J.C. *Atomic Data and Nuclear Data Tables*, **54** (2), 181 (1993); http://henke.lbl.gov/optical_constants/.
9. Yoshikawa I., Murachi T., Takenaka H., Ichimaru S. *Rev. Sci. Instrum.*, **76**, 066109 (2005).
10. Hotta Y., Furudate M., Yamamoto M., Watanabe M. *Surf. Rev. Lett.*, **9** (1), 571 (2002).
11. Zuev S.Yu., Polkovnikov V.N., Salashchenko N.N. *Proc. XIIth Intern. Nanophys. Nanoelectron. Symp.* (N. Novgorod, 2008) Vol. 1, p. 227.
12. Codling K., Madden R.P. *Phys. Rev.*, **167** (3), 587 (1968).
13. Gahwiller C., Brown F.C. *Phys. Rev. B*, **2** (6), 1918 (1970).
14. Mitrofanov A.V., Zuev S.Yu. *Izv. Ross. Akad. Nauk, Ser. Fiz.*, **68** (4), 556 (2004).